Formation of Optical Subcycle Pulses and Full Maxwell-Bloch Solitary Waves by Coherent Propagation Effects

V. P. Kalosha* and J. Herrmann

Max-Born-Institute for Nonlinear Optics and Short Pulse Spectroscopy, Rudower Chaussee 6, 12489 Berlin, Germany

(Received 25 November 1998)

We demonstrated that optical subcycle pulses can be generated in dense media of two-level systems due to pulse splitting and reshaping of pulses of a few optical-cycles time duration. Novel features in the spectral signatures of the pulses are predicted, a large blueshift in the transmitted and a large redshift in the reflected pulse, which are explained by intrapulse four-wave mixing. Solitary propagation phenomena in the full Maxwell-Bloch equations beyond the limits of slowly varying envelope and rotating-wave approximations are observed, e.g., the formation of solitary half-cycle pulses and two-soliton pulses.

PACS numbers: 42.65.Re, 42.50.Gy

Recent advances in ultrafast laser technology have made possible the generation of extremely short and intense pulses with only two optical periods or less than 5 fs in duration in the visible region [1,2]. Efforts for generation of still shorter pulses are motivated by the possibility to study light-matter interactions under unique conditions as the pulse duration approaches the duration of a single optical cycle. Subcycle pulses represent a new type of radiation, which is now quasistatic in nature because of the absence of a fast-oscillating ac component. Such intense pulses will bring a vast variety of intriguing new physical phenomena in the light-matter interaction and provide a large potential of possible applications.

Currently, subcycle pulses are available only in the spectral region of THz with a duration of about 0.5 ps [3]. The duration of pulses generated directly from a mode-locked solid-state laser is limited by a number of physical effects such as dispersion control over the whole spectrum and a limited gain bandwidth. In the most frequently used method of pulse shortening, a nonlinear waveguide for spectral broadening and linear dispersive optical elements for the compensation of the frequency-depending phase are utilized [2]. However, with the extremely increased bandwidth of subcycle pulses, such dispersion control is difficult to realize. Several other potential techniques have been proposed recently. Most interesting are proposals to reach the sub-fs limit by high-harmonic generation that relies on phase locking between consecutive harmonics or utilizes single harmonics [4]. Another approach uses the interaction of THz subpicosecond half-cycle pulses with two-level atoms [5].

The most promising conditions for the generation of sub-fs pulses are provided by strong nonlinear processes with a high degree of the spatiotemporal coherence. We investigated such a process whereby a layer of a resonant dense medium described by a two-level model is driven by a strong and extremely short optical pulse. For pulses with a duration of many cycles, the nonlinear properties of two-level media have been studied in a large number of papers. In particular, the resonant interaction of pulses shorter than all relevant relaxation times of the medium gives rise to the effect of self-induced transparency (SIT) and pulse splitting [6]. It is based on the slowly varying amplitude approximation (SVEA) of Maxwell's equations and the rotating-wave approximation (RWA) of the density matrix equation. Clearly, these approximations fail if the pulse duration approaches the duration of several optical cycles [7–9]. Here we explore such a propagation regime and solve the full Maxwell equations and the full Bloch equations without the use of SVEA or RWA.

We consider the propagation of an extremely short pulse along the z axis normally to an input interface of a resonant two-level medium at $z = 0$. Initially the pulse moves in the free space; then it partially penetrates into the medium and partially reflects backwards; the penetrating part propagates through the medium and finally exits again into the free space through the output interface at $z = L$. With the constitutive relation for the electric displacement for linear polarization along the x axis, $D_x = \epsilon_0 E_x + P_x$, the Rabi frequency $\Omega = dE_x/\hbar$ and $\Psi = \sqrt{\mu_0/\epsilon_0}\, dH_y/\hbar$ Maxwell's equations for the medium take the form

$$\dot{\Psi} = -\frac{\partial \Omega}{\partial \zeta}, \qquad \dot{\Omega} + \omega_c \dot{u} = -\frac{\partial \Psi}{\partial \zeta}, \tag{1}$$

where an overdot signifies a time derivative, E_x, H_y are the electric and magnetic fields, respectively, d is the dipole moment, $\zeta = z/c$, $\omega_c = Nd^2/\epsilon_0\hbar$, and N is the density. In Eqs. (1) the macroscopic nonlinear polarization $P_x = N\, du$ is connected with the off-diagonal density matrix element $\rho_{12} = \frac{1}{2}(u + iv)$ and the population difference $w = \rho_{22} - \rho_{11}$, which are determined by the Bloch equations [6]:

$$\begin{aligned} \dot{\rho}_{12} + (\gamma_2 - i\omega_0)\rho_{12} &= i\Omega w, \\ \dot{w} + \gamma_1(w + 1) &= -2\Omega v. \end{aligned} \tag{2}$$

Here ω_0 is the resonant frequency, and γ_1 and γ_2 are, respectively, the population and polarization relaxation

 0031-9007/99/83(3)/544(4)$15.00

constants. The initial condition is $\Omega(t = 0, \zeta) = \Psi(t = 0, \zeta) = \Omega_0 \cos[\omega_p(\zeta - \zeta_0)]\,\mathrm{sech}[1.76(\zeta - \zeta_0)/\tau_p]$, where Ω_0 is the peak Rabi frequency of the incident pulse, ω_p is the carrier frequency, and τ_p is the FWHM of the pulse intensity envelope. The choice of ζ_0 ensures that the pulse penetrates negligibly into the medium at $t = 0$. The medium is initialized with $u = v = 0$ and $w = -1$ at $t = 0$.

Note that Maxwell's equations in the normalized form (1) show the role of the collective frequency parameter ω_c as a measure of the coupling between the field and the medium. Assuming the resonance condition $\omega_p = \omega_0$ and slow relaxation times, the solution of the problem depends only on three normalized parameters $\Omega_0\tau_p$, $\omega_c\tau_p$, and $\omega_0\tau_p$ which permit a rescaling of the five atomic and pulse parameters. Several gaseous atoms have well isolated resonances in the optical region (as, e.g., rubidium with $\omega_p = 2.4\ \mathrm{fs}^{-1}$), but the necessary high density or high pressure for the required parameters as given below is scarcely to realize. However, the two-level model can be still applied for the description of coherent effects for materials with a broad distribution of transitions such as inhomogeneously broadened resonance lines in gases and solids [6], but also in the sense of an approximation for inhomogeneous quasicontinuous energy bands as, e.g., in semiconductors [10,11]. In these more complex systems the coherent superposition of a band of continuous transitions with approximately the same dipole moment manifests like a unified single level with an inhomogeneous linewidth $(T_2^*)^{-1}$. In the present Letter the inhomogeneous broadening is neglected. In the following we consider the dimensionless parameters of the problem in the ranges $\omega_0\tau_p = 11.5$, $1 \le \omega_c\tau_p \le 10$, $7 \le \Omega_0\tau_p \le 22$. It is instructive to indicate concrete initial pulse and material parameters which meet these conditions: $\tau_p = 5$ fs, $\omega_p = \omega_0 = 2.3\ \mathrm{fs}^{-1}$ ($\lambda = 830$ nm), $d = 2 \times 10^{-29}$ A s m, $\gamma_1^{-1} = 1$ ps, $\gamma_2^{-1} = 0.5$ ps. For these parameters the density $N = 4.4 \times 10^{20}\ \mathrm{cm}^{-3}$ gives $\omega_c = 0.2\ \mathrm{fs}^{-1}$ and the Rabi frequency $\Omega_0 = 1\ \mathrm{fs}^{-1}$ corresponds to the electric field of $E_x = 5 \times 10^9$ V/m or an intensity of $I = 6.6 \times 10^{12}\ \mathrm{W/cm}^2$.

Equations (1) and (2) were integrated by use of Yee's finite-difference time-domain (FDTD) discretization scheme [12] for the fields and the predictor-corrector method for the material variables [7]. Nonreflecting boundary conditions [13] were incorporated with FDTD discretization which avoids the influence of the finite-space computational domain. The performance of the numerical scheme was monitored at each time update by calculation of the pulse energy, the energy stored in the medium, and the energy flux through the computational-domain boundaries in comparison with the energy of the initial pulse. In all of our simulations the total energy was conserved with an accuracy better than 0.001%.

We have obtained solutions of Eqs. (1) and (2) for different input pulse parameters and medium densities. In general, with an input envelope area $\mathcal{A} = 1.76\Omega_0\tau_p$ smaller than π and chosen medium densities, the main part of the pulse is reflected, but with increasing area splitting of the penetrating part accompanied by pulse shortening occurs, in agreement with results within the SVEA and RWA [6]. However, in detail the pulse evolution dramatically changes for input pulses with a duration of 5 to 10 fs, where novel transient features arise which qualitatively differ from standard results. As an example, in Fig. 1 the reflected, penetrating, and transmitted pulses are shown for different medium densities and a fixed input pulse maximum $\Omega_0 = 1.4\ \mathrm{fs}^{-1}$ corresponding to the envelope area $\mathcal{A} = 4\pi$. For the case of lower density with $\omega_c = 0.2\ \mathrm{fs}^{-1}$, the reflection is weak and the penetrating part is strong enough to split into two pulses, the stronger of which moves faster than the weaker. In the case of a more dense medium (Fig. 1b), a significant part of radiation with low-frequency oscillations on the back front is reflected from the boundary. With further propagation the pulses in Fig. 1 behave in a different manner. For the less dense medium the weaker pulse in Fig. 1(a) decays quickly, while the first pulse propagates over much longer distances. In Fig. 2 pulse shape, polarization and population inside the medium with $\omega_c = 0.2\ \mathrm{fs}^{-1}$ is shown at a propagation distance of $z = 27\ \mu$m. As seen in comparison with the incident pulse (dotted line), the pulse is significantly shortened up to almost a single cycle, the population is completely inverted in the pulse peak and driven back to the ground level at pulse back front, and the polarization has the same direction as the field; nevertheless, the evolution does not lead to a solitary propagation regime. In comparison, for the higher density with $\omega_c = 1\ \mathrm{fs}^{-1}$ the electric field, polarization and population at $z = 60\ \mu$m are shown in Fig. 3. In this case we observe a few-cycle field oscillating with higher frequency as compared with the initial pulse oscillations. The polarization follows the field quite accurately in time, but with opposite direction. As a consequence the phase

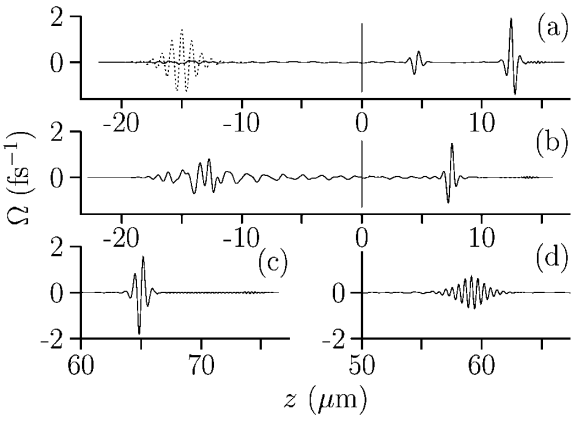

FIG. 1. Electric field profiles for different time moments and medium densities near the input face [(a),(b)] and outside the exit face [(c),(d)]. Parameters: $\Omega_0 = 1.4\ \mathrm{fs}^{-1}$, $L = 45\ \mu$m; (a) $t = 0.1$ ps, $\omega_c = 0.2\ \mathrm{fs}^{-1}$; (b) $t = 0.1$ ps, $\omega_c = 1\ \mathrm{fs}^{-1}$; (c) $t = 0.3$ ps, $\omega_c = 0.2\ \mathrm{fs}^{-1}$; (d) $t = 0.4$ ps, $\omega_c = 1\ \mathrm{fs}^{-1}$. Dotted line: Incident pulse at $t = 0$.

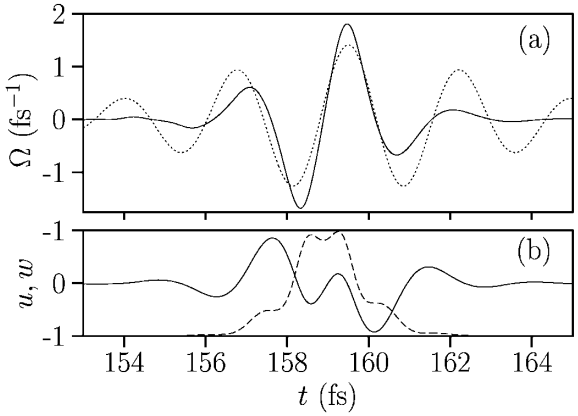

FIG. 2. (a) Temporal shape of the electric field (solid line); (b) polarization u (solid line) and population w (dashed line) at $z = 27$ μm inside the medium for $\omega_c = 0.2$ fs^{-1}, $\Omega_0 = 1.4$ fs^{-1}, $L = 45$ μm. The incident pulse shifted to the same peak position is shown by the dotted line.

velocity of this pulse is larger than the light velocity in free space. It is remarkable that in this case the pulse propagation and the two-level atom dynamics show evidence of a soliton propagation regime beyond SVEA and RWA which will be discussed later.

To expose the carrier frequency changes in detail, we present in Fig. 4 the evolution of the pulse spectrum during propagation through a 150-μm thick layer for the case $\omega_c = 1$ fs^{-1} and $\Omega_0 = 1.4$ fs^{-1}. As seen the reflected pulse consists of two separated portions. One peak is located around the input central frequency ω_0, while the other part shows a large redshift with a spectrum maximum position at approximately $0.5\omega_0$. On the other hand, the main part of the penetrating pulse spectrum exhibits a blueshift with a maximum at $1.5\omega_0$.

The physical interpretation of the observed spectral transformation during the propagation can be given by intrapulse third-order four-wave mixing (FWM) of the type $2\omega \rightarrow \omega' + \omega''$ with ω being the pulse component frequency within the bandwidth and ω' and ω'' the new resulting frequencies. Such a nonlinear process is ignored in the framework of RWA, but it is clearly presented in the exact Bloch equations and becomes significant for very short pulses. Significant FWM occurs only if the phase-matching condition $\Delta k + \Delta k_{nl} = 0$ is satisfied, where Δk_{nl} is due to a nonlinear contribution in the Bloch equations (2). The z-depending maximum shift and spectral broadening in Fig. 4 can be explained from the solution of this phase-matching condition with $\Delta k = 2k(\omega) - k(\omega') - k(\omega'')$ for collinear forward propagation and $\Delta k = -2k(\omega) - k(\omega') - k(\omega'')$ for backward propagation with the linear dispersion relation in the limit of weak medium excitation (which is the case in Figs. 3 and 4) $k(\omega) = (\omega/c)\Re\sqrt{1 + \omega_c/(\omega_0 - \omega + i\gamma_2)}$.

Note that for longer pulses with $\gamma_2^{-1} \ll \tau_p \ll \gamma_1^{-1}$ another type of frequency transformation in two-level systems with a much smaller redshift in the reflected wave has been predicted in Ref. [14]. At these conditions a saturable absorption front is formed in the medium, and the redshift due to self-reflection from this moving front has been explained by the Doppler effect.

In Fig. 5 we present the propagation of a more intense incident pulse with the Rabi frequency $\Omega_0 = 4.4$ fs^{-1} and the envelope area $\mathcal{A} = 12.5\pi$ in a more dense medium with $\omega_c = 2$ fs^{-1}. In this case the reflected pulse is rather weak and the penetrating part splits mainly into three pulses with different field strengths and velocities. With further propagation these pulses evolve into a higher-frequency oscillating pulse and two separated half-cycle pulses of opposite polarity. Both unipolar half-cycle pulses with a duration <1 fs are not attenuated during long-term propagation and show a clear solitary behavior. As remarked above the existence of SIT solutions of the envelope equations is restricted by the validity of SVEA and RWA, which is violated for the conditions considered here. However, there exists an exact nonoscillating solitary solution for field strength of the full Maxwell-Bloch equations (1) and (2) (with $\gamma_1 = \gamma_2 = 0$), which

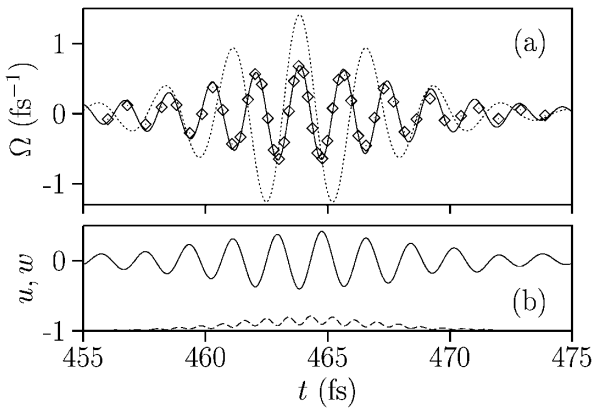

FIG. 3. As in Fig. 2 but for $z = 60$ μm, $\omega_c = 1$ fs^{-1}, $L = 150$ μm. Diamonds represent the solution (4).

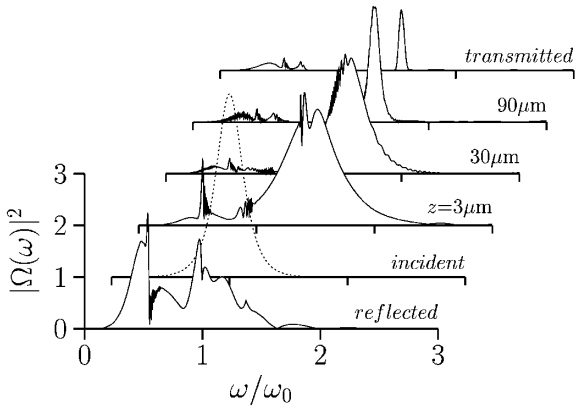

FIG. 4. Evolution of the pulse spectrum during propagation inside and outside the medium for $\omega_c = 1$ fs^{-1}, $\Omega_0 = 1.4$ fs^{-1}, $L = 150$ μm.

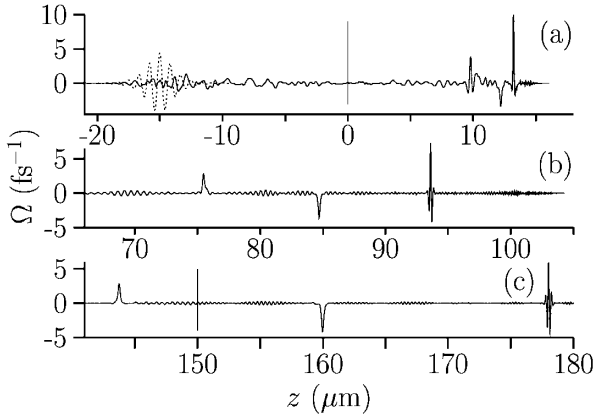

FIG. 5. Electric field profiles near the input face located at $z = 0$ (a), inside the medium (b), and near the output face located at $z = 150$ μm (c) for $\omega_c = 2$ fs^{-1}, $\Omega_0 = 4.4$ fs^{-1}. (a) $t = 0.1$ ps; (b) $t = 0.4$ ps; (c) $t = 0.7$ ps. The incident pulse at $t = 0$ is shown by the dotted line.

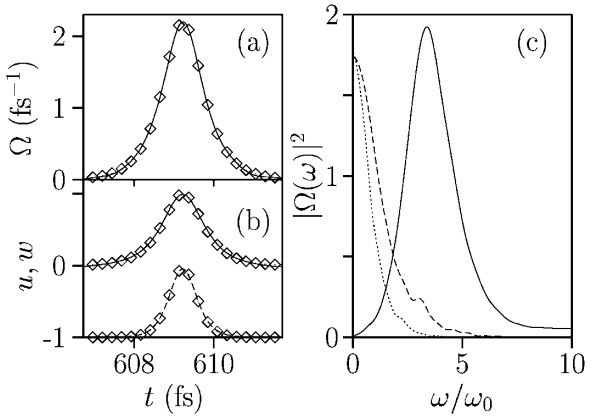

FIG. 6. (a) Temporal shape of the electric field, (b) polarization (solid line) and population (dashed line) at $z = 120$ μm for $\omega_c = 2$ fs^{-1}, $\Omega_0 = 4.4$ fs^{-1}, $L = 150$ μm. Diamonds represent the solution (3). (c) Spectrum of the first high-frequency pulse (solid line), second (long-dashed line), and third (short-dashed line) unipolar pulses at $z = 120$ μm.

is given by the expressions

$$\Omega = A\,\mathrm{sech}[A(t - m\zeta)], \qquad u = 2\omega_0\beta\Omega\,,$$
$$w = -1 + 2\beta\Omega^2, \tag{3}$$

where $m = \sqrt{1 + \beta\omega_0\omega_c}$ is the pulse refractive index and $\beta = (A^2 + \omega_0^2)^{-1}$ [15]. The solution (3) describes a unipolar half-cycle pulse with the amplitude A that is the only free parameter determining the pulse duration. As shown in Fig. 6 for the third pulse of Fig. 5 the numerically obtained solutions and the solution (3) being fitted only by the amplitude can be clearly identified with each other even though the pulse propagation in Fig. 5 at $z = 120$ μm is still not completely in a steady-state regime because the three pulses still interact. In Fig. 6c the spectra of the three pulses are presented. As expected both half-cycle pulses show extended spectra up to zeroth frequencies, while the first pulse has a large blueshift of the carrier frequency with a mean frequency $\bar{\omega} \approx 4\omega_0$.

Note that the fastest blueshifted pulse in Fig. 5 shows also a solitary behavior but, in difference to the half-cycle pulses, that of a multisoliton solution. Far away from the input interface, Maxwell's equations can be approximated by a reduced version without the use of SVEA and RWA, but with the neglect of back reflection. These reduced Maxwell-Bloch equations have exact multisoliton solutions [16]. Their two-soliton solution describing a localized pulse with "internal" oscillations is given by

$$\Omega = A\,\mathrm{sech}\,\vartheta_e \frac{\cos\vartheta - \alpha\sin\vartheta\tanh\vartheta_e}{1 + \alpha^2\sin^2\vartheta\,\mathrm{sech}^2\vartheta_e}\,, \tag{4}$$

where the amplitude A and carrier frequency $\bar{\omega}$ are free parameters, $\vartheta_e = A(t - m_e\zeta)/2$, $\vartheta = \bar{\omega}(t - m\zeta)$, $\alpha = A/2\bar{\omega}$. The refractive indices m_e, m and the atomic variables are given in Ref. [16]. The solution (4) with $\bar{\omega} = \int_0^\infty \omega|\Omega(\omega)|^2\,d\omega / \int_0^\infty |\Omega(\omega)|^2\,d\omega$ and an appropriate choice of the amplitude coincides well with the blueshifted pulse fields found numerically for both cases of high medium density in Figs. 3 and 5. The direct comparison of analytical and numerical solutions for $\omega_c = 1$ fs^{-1} is shown by diamonds in Fig. 3.

We thank Dr. M. Müller for constructive discussions and suggestions. We acknowledge partial support of this work by BMBF, Project No. WEI-001-98, and INTAS, Project No. 97-2018.

*Also at Institute for Nuclear Problems, Belarus State University, Minsk, Belarus.
Email address: kalosha@mbi-berlin.de

[1] J. Zhou *et al.*, Opt. Lett. **19**, 1149 (1994); A. Stingel *et al.*, Opt. Lett. **20**, 602 (1995).
[2] M. Nisoli *et al.*, Opt. Lett. **22**, 522 (1997).
[3] R. R. Jones, D. You, and P. H. Bucksbaum, Phys. Rev. Lett. **70**, 1236 (1993).
[4] G. Farcas and C. Toth, Phys. Lett. A **168**, 447 (1992); P. Antoine, A. L'Huillier, and M. Lewenstein, Phys. Rev. Lett. **77**, 1234 (1996).
[5] A. E. Kaplan and P. L. Shkolnikov, Phys. Rev. Lett. **75**, 2316 (1995).
[6] L. Allen and J. H. Eberly, *Optical Resonance and Two-Level Atoms* (Wiley, New York, 1975).
[7] R. W. Ziolkowski, J. M. Arnold, and D. M. Gogny, Phys. Rev. A **52**, 3082 (1995).
[8] M. Müller, V. P. Kalosha, and J. Herrmann, Phys. Rev. A **58**, 1372 (1998).
[9] S. Hughes, Phys. Rev. Lett. **81**, 3363 (1998).
[10] H. Haug and S. W. Koch, *Quantum Theory of the Optical and Electronic Properties of Semiconductors* (World Scientific, Singapore, 1993), 2nd ed.
[11] V. P. Kalosha, M. Müller, and J. Herrmann, J. Opt. Soc. Am. B **16**, 323 (1999).
[12] K. S. Yee, IEEE Trans. Antennas Propag. **14**, 302 (1966).
[13] E. L. Lindman, J. Comput. Phys. **18**, 66 (1975).
[14] W. Forysiak *et al.*, Phys. Rev. Lett. **76**, 3695 (1996).
[15] R. K. Bullough and F. Ahmad, Phys. Rev. Lett. **27**, 330 (1971).
[16] J. C. Eilbeck *et al.*, J. Phys. A **6**, 1337 (1973).